An Effective Model-free Predictive Current Control for Synchronous Reluctance Motor Drives

P.G. Carlet, F. Tinazzi, *Member*, *IEEE*, S. Bolognani, *Fellow Member*, *IEEE*, and M. Zigliotto, *Senior Member*, *IEEE*

***Abstract*—The performances of a model predictive control (MPC) algorithm largely depend on the knowledge of the system model. A model-free predictive control approach skips all the effects of parameters variations or mismatches, as well as of model nonlinearity and uncertainties. A finite-set model-free current predictive control is proposed in this paper. The current variations predictions induced by the eight base inverter voltage vectors are estimated by means of the previous measurements stored into look-up tables. To keep the current variations information up to date, the three current measurements due to the three most recent feeding voltages are combined together to reconstruct all the others. The reconstruction is performed by taking advantage of the relationships between the three different base voltage vectors involved in the process. In particular, 210 possible combinations of three-state voltage vectors can be found, but they can be gathered together in six different groups. A light and computationally fast algorithm for the group identification is proposed in this paper. Finally, the current reconstruction for the prediction of future steps is thoroughly analysed. A compensation of the motor rotation effect on the input voltages is proposed, too. The control scheme is evaluated by means of both simulation and experimental evidences on two different synchronous reluctance motors.**

***Index Terms*—Synchronous reluctance motor, model predictive control, MPC, model-free, variable speed drives.**

I. Introduction

Model predictive control has been widely investigated and implemented in different fields [1], [2]. It is based on the prediction of the system future reaction to the control inputs and the subsequent selection of the optimal control action, based on the minimisation of a given cost function.

In particular, MPC has been successfully applied to electric drives. Many MPC current control schemes have been developed for different kinds of synchronous electric motors, such as surface [3] and interior permanent magnet motors [4] or synchronous reluctance motors (SynRM) [5].

MPC schemes are classified in Finite Control Set (FCS) or Convex Control Set (CCS), depending on how the optimum voltages are generated. The former use only the base inverter space voltage set [6]. In case of a motor fed by a three-phase two levels inverter, the number of voltage vectors in the set is eight. Thanks to a low number of set elements, the optimum detection is fast, provided that a short prediction horizon is considered. The computational burden increases exponentially as more than two future time steps are used as horizon length. On the other hand, in a CCS solution the optimum voltages are generated by a linear combination of the inverter base vectors set. In this latter case, optimum is computed solving a quadratic-programming tracking problem, which usually requires a high computational effort.

In model-based predictive current control schemes the current predictions are based on the state-space model of the system, conveniently written in a dq reference frame synchronous to the rotor flux. The prediction accuracy is strongly influenced by the knowledge of the parameters, for which several identification techniques are available [7]–[10].

Several approximations are commonly introduced to simplify the system description, such as linear magnetic flux-current characteristics, constant stator resistance and absence of magnetic cross-coupling between the direct and quadrature axes. As a consequence, parameter mismatches always affect the model, because of the electric load changes induced by either the iron-saturation (particularly evident in SynR motors) or the temperature variation. Parameters mismatch can be reduced by the use of observers, which anyway pose the problem of convergence, stability and accuracy. Online parameter tracking also improves any model-based scheme, at the price of higher computational and tuning efforts.

A different approach is considered in this work. The conventional description of the system is abandoned, moving to a model-free concept firstly introduced by Lin et al. [11]. The motor current variations caused by the application of each of the eight inverter base voltage vectors over a switching interval are stored in two look-up tables (LUTs), one for each axis. The LUTs content is continuously updated online. A key parameter of a model-free predictive current control is the LUTs update frequency.

If the frequency is too low, the scheme suffers of *stagnation* problem, described in [12]. In a nutshell, if a voltage vector is not applied for many consecutive time steps, the stored information regarding the related current variation is obsolete and unreliable. Long stagnation periods could compromise even the system stability.

In order to avoid stagnation, several methods have been presented. They can be divided in two groups: *direct* and *indirect* anti-stagnation methods. A first simple, but bulky, method for increasing the update frequency is obtained with the direct anti-stagnation algorithm proposed by the same authors in [12]. A minimum refresh frequency is imposed for the current LUTs. If one of the base voltages is not applied for a predefined time window, the voltage vector is forcedly imposed as next voltage reference. In other words, MPC

P.G. Carlet and S. Bolognani are with the Dept. of Industrial Engineering, University of Padova, 35131 Padova, Italy (e-mail: paologherardo.carlet@studenti.unipd.it, silverio.bolognani@unipd.it).

F. Tinazzi and M. Zigliotto are with Dept. of Management and Engineering, University of Padova, Stradella S. Nicola 3, Vicenza 36100, Italy. (e-mail: {fabio.tinazzi, mauro.zigliotto}@unipd.it

optimum detection is neglected and the updated information is retrieved at the cost of an increase of the current ripple.

A smart anti-stagnation algorithm is proposed in [13], where an indirect LUTs reconstruction is presented. Current LUT update is based on the mathematical relationships that link the inverter input voltages. The knowledge of the last three current variations permits an approximated update of the other LUTs elements. The update is obtained without penalising the current ripple as in [12], since the updating frequency is high enough to prevent stagnations. Furthermore, the current ripple and the update frequency are not so strictly linked, as in the previous model-free predictive control solutions [11], [12].

This paper presents a novel algorithm which further increases the updating frequency of the LUTs, while maintaining the cost function minimisation and by taking advantage only on the past current measurements. The LUTs update is guaranteed after each current measurement and it skips any stagnation completely.

The scope of our work is to avoid the need of the motor model, rather than proposing a predictive control method with better performances (in terms of dynamics and prediction error) with respect to the existing model-based ones. This is a particularly valuable feature for plug-and-play drives connected to motors with few or no parameters available. Examples are general purpose drives and ac drives for compressors adopted in cooling equipment (sometimes the motor is not accessible at all). In this light, the model-free predictive control is a promising control strategy for electric motors and it is worth attention from researchers.

The paper is organised as follows. The theory of operations of the model-free predictive current control is presented in Sec. II, whereas the innovative updating strategy is explained in Sec. III. The simulation and experimental results are reported and discussed in Sec. IV.

II. Theory of predictive current control

The idea underlying the model predictive current control is to predict the future behaviour of the system and to choose the input voltage vector that minimises the cost function J defined as follows:

$$J = \|\mathbf{i}^*_{dq} - \widehat{\mathbf{i}}^z_{dq}(k+N)\|^2 \qquad z \in [0,\dots,6] \tag{1}$$

where the prediction horizon, expressed in number of control periods T_c, is fixed to $N = 2$ in the present proposal. $\mathbf{i}^*_{dq} = \left[i^*_d; i^*_q\right]$ is the reference current vector and $\widehat{\mathbf{i}}^z_{dq} = [\widehat{i}_d; \widehat{i}_q]$ is the dq vector of the predicted current due to one of the eight base inverter voltage vectors $\mathbf{u}^z$:

$$\begin{cases} \mathbf{u}^z & = \frac{2}{3} U_{\text{dc}} e^{j\frac{\pi}{3}(z-1)} \qquad z \in [1,\dots,6] \\ \mathbf{u}^z & = 0 \qquad\qquad\qquad\qquad\quad z = 0 \end{cases} \tag{2}$$

where U_{dc} is the inverter bus voltage.

Eq. (1) is the simplest quadratic cost function that can be adopted in a reference tracking problem. Of course, more complex cost functions can be adopted at the price of a higher computational load and an additional tuning of cost function gains [14], [15]. For instance, a thermal stress based MPC was implemented in [16].

However, the performance of a model predictive current control depends on the current prediction accuracy, which is the topic of this paper. In this light, the adoption of (1) seems appropriate, since it allows a fair comparison with other predictive control techniques. For the sake of lighter mathematical notations, the reference frame dq subscripts as well as the time dependence will be omitted hereinafter.

The compete model of the SynRM is given by

$$\frac{d\mathbf{i}}{dt} = \begin{bmatrix} l_d & l_{dq} \\ l_{dq} & l_q \end{bmatrix}^{-1} \left(\mathbf{u} - R\mathbf{i} - \omega_{\text{me}} \begin{bmatrix} 0 & -L_q \\ L_d & 0 \end{bmatrix} \mathbf{i} \right) \tag{3}$$

where $\mathbf{u}$ is the phase voltage vector applied to the motor, $\mathbf{i}$ the current phase vector. The parameters are the stator resistance R, the dq apparent inductances L_d, L_q, the differential inductances l_d,l_q and the cross-differential inductances $l_{dq} = l_{qd}$.

It is worth noting the parameters in (3) are time varying and depend on the working point. The motor magnetic flux linkages may suffer of severe saturation effects as the example in Fig. 1. Therefore, a specific motor characterisation is required to achieve a correct system model, which usually implies laboratory tests and data post-processing.

In the model-based control, the expression of a current variation is written as follows:

$$\Delta\mathbf{i}^z(k+1) = \mathbf{A}\mathbf{i}(k) + \mathbf{B}\mathbf{u}^z(k) \tag{4}$$

Matrices $\mathbf{A}$ and $\mathbf{B}$ are easily derived from (3) and they contain all the SynR motor parameters.

Opposite to model-based control, the proposed model-free algorithm uses only the current measurements without information about motor parameters. Each of the seven base voltage vectors, if applied, results in current variations on both d and q axes that can be stored in two different LUTs. The seven current variations at time step k due to the seven voltage vectors are supposed to be known and actual:

$$\mathbf{i}(k) - \mathbf{i}(k-1) = \Delta\mathbf{i}^z(k) \tag{5}$$

According to the finite control set policy, the cost function (1) is evaluated seven times at each control period. The next-step currents are estimated as follows:

$$\begin{aligned} \widehat{\mathbf{i}}^z(k+1) &= \mathbf{i}(k) + \Delta\mathbf{i}^z(k) \\ \widehat{\mathbf{i}}^z(k+2) &= \widehat{\mathbf{i}}^z(k+1) + \Delta\mathbf{i}^z(k+1) \end{aligned} \tag{6}$$

where $\mathbf{i}(k)$ are the current measurements at time k and $\Delta\mathbf{i}^z(k)$ is the current variation due to the vector $\mathbf{u}^z(k)$ which has been already decided at time $(k-1)$. The voltage vector to be applied at time $(k+1)$ is selected by means of (1).

Each of the current variations in (5) can be split in two components:

$$\Delta\mathbf{i}^z(k) = \delta\mathbf{i}^0(k) + \delta\mathbf{i}^z(k) \tag{7}$$

where $\delta\mathbf{i}^0 = [\delta i^0_d; \delta i^0_q]$ is the natural response and $\delta\mathbf{i}^z = [\delta i^z_d; \delta i^z_q]$ is the forced response to an active voltage vector $\mathbf{u}^z$. In case of $\mathbf{u}^0$, it is straightforward that $\Delta\mathbf{i}^0 = \delta\mathbf{i}^0$.

Since the values of $\Delta\mathbf{i}^z$ are obtained from measurement, they inherently contain information about the real behaviour of the SynRM close to the actual working point. Fig. 2 shows an example of current variations $\delta\mathbf{i}^z(k),\ z \in [1\dots6]$, relative

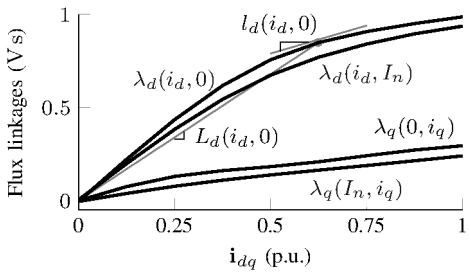

Fig. 1. Magnetic flux linkages of a SynRM at different currents and an example of d-axis apparent L_d and differential l_d inductances.

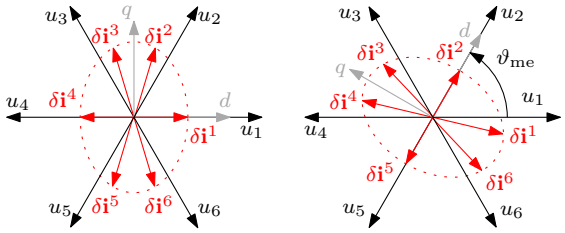

Fig. 2. Current variations $\delta\mathbf{i}^z$ in a SynRM with the six active vectors $\mathbf{u}^z$ at different rotor position: $\vartheta_{\text{me}} = 0$ (left) and $\vartheta_{\text{me}} = \pi/3$ (right).

to two different rotor positions. For simplicity, it is assumed $\mathbf{i}(k) = 0$. Due to the anisotropy of the SynRM, the same active voltage vectors induce different current variations, depending on the rotor position ϑ_{me}. In general, it is $\Delta\mathbf{i}^z = f(\mathbf{i}, z, \vartheta_{\text{me}})$. Similarly, the current variations associated to the natural response depends on the actual currents and the motor back-electromotive force, i.e. the speed ω_{me}, so that $\delta\mathbf{i}^0 = f(\mathbf{i}, \omega_{\text{me}})$.

The LUTs content should be updated with the highest possible frequency to assure that the stored current variations return reliable information about the actual working point of the SynRM. However, only one voltage vector per control period step can be applied with a finite-set model predictive control algorithm. It implies that only one pair of current measurement variations $\Delta\mathbf{i}$ stored in the LUTs can be updated based on the latest current measurement. For the sake of current prediction accuracy, the remaining six pairs of $\Delta\mathbf{i}$ should be updated with a different strategy.

III. The Updating of the Current Variations LUTs

As mentioned above, a possible drawback of the model-free approach is the *stagnation* effect [12], [13]. It happens when one (or more) element of the LUTs are not updated for many

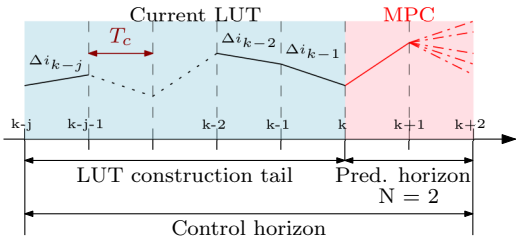

Fig. 3. Discrete time representation of the control horizon.

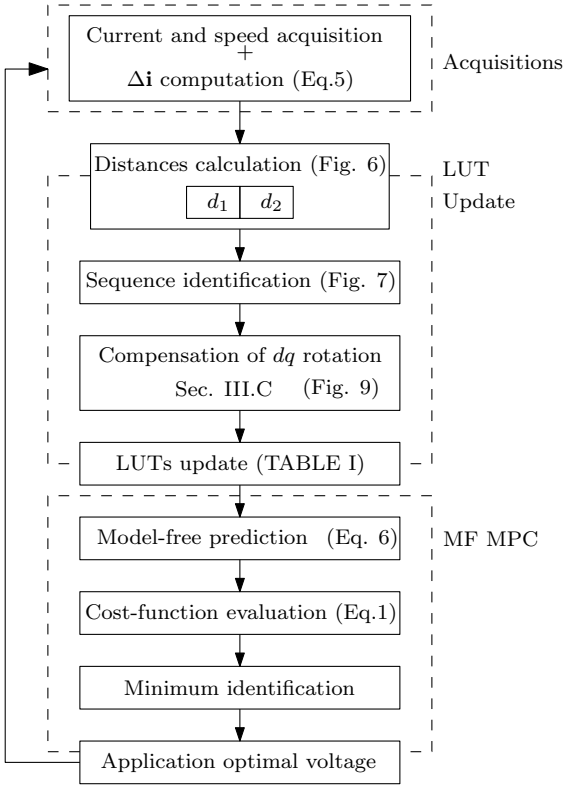

Fig. 4. Sequence of operations at every control cycle.

time steps, which means that a voltage vector has not been used for several switching cycles.

The finite-set algorithm applies just one (out of seven) base voltage vector for an entire control period T_c. The anti-stagnation solution proposed in [13], [17] uses the current variations relative to the last three periods to reconstruct all the other (older) four ones. A weak point is that the reconstructions are made for use in the prediction horizon time span, when the rotor electrical position ϑ_{me} may have changed.

There are also a couple of possible situations that can corrupt the mechanism. The first case is when only two voltage vectors are applied for a long interval and thus only two couple of LUTs elements are actually updated. Even worse the second case, when only one vector is applied. These two cases may prevent a stable length of the LUTs construction tail (see Fig. 3). The problem of the stagnation, i.e. the lengthening of the LUTs construction tail, was quite evident since the very beginning. A constant tail length was guaranteed in the seminal paper [12] at the price of non-optimal base voltage vector choices, which cause current ripple inhomogeneities.

This paper aims at fixing the weak points outlined above, as an indispensable improvement for the practical application of the model-free control paradigm. In a nutshell, the goal is to maximise the updating frequency of the current variations $\Delta\mathbf{i}^z$. The goal can be obtained by the method proposed in Sec. III-A and III-B. Furthermore, the rotor electrical position variation can be accounted for as explained in Sec. III-C. The whole updating process as well as the prediction algorithm is summarised by the flow-chart reported in Fig. 4.

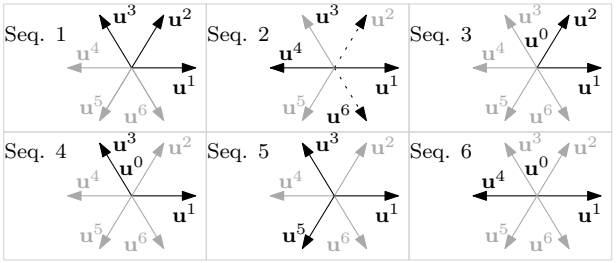

Fig. 5. Voltage vector sequences. The rotation by multiples of $\pi/3$ of the selected (black) vectors returns the same sequence type. Dotted vectors in sequence 2 means that the sequence is obtained by either vector $\mathbf{u}^2$ or $\mathbf{u}^6$.

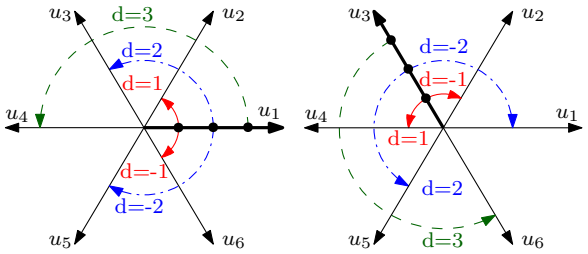

Fig. 6. Examples of angular displacement and distance d calculation between active vectors. Reference vectors are $\mathbf{u}^1$ (left) and $\mathbf{u}^3$ (right), respectively.

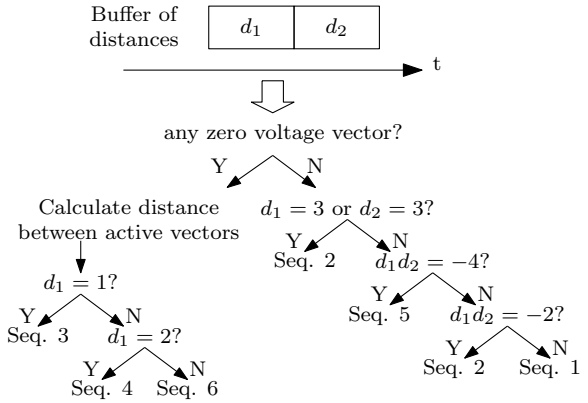

Fig. 7. Sequence identification based on the buffer distances.

A. The voltage triplet identification

The proposed LUTs update method is based on the identification of particular combinations of three different voltage vectors referred to as *triplet*, whereas the specific combination they form is called *sequence*.

Six sequences can be defined as shown in Fig. 5. It is important to underline that the highlighted vectors are just examples to graphically define the sequences. For instance, sequence 1 is formed by either the vectors $(1, 2, 3)$ or $(2, 3, 1)$, as well as $(3, 1, 2)$. Furthermore, sequence 1 is formed by either the vectors $(3, 4, 5)$ or $(5, 6, 1)$, including all the possible permutations.

The sequences can be used to define mathematical relationships that allow to reconstruct the four current variations due to the remaining four voltage vectors, as it is reported in Sec. III-B. A practical example is also reported in [17]. Since the current reconstructions depends on the sequence type, it is convenient to define an algorithm for the sequence identification.

The first step of the solution proposed in this paper consists in defining a buffer $B_u = [\mathbf{u}^z(t_3); \mathbf{u}^z(t_2); \mathbf{u}^z(t_1)]$ containing the last three applied voltage vectors, where $\mathbf{u}^z(t_1)$ corresponds to the latest applied voltage vector and $\mathbf{u}^z(t_3)$ to the oldest one, that is $t_3 < t_2 < t_1$. The buffer is updated by following two rules:

- the three voltage vectors must be different;
- the buffer is time oriented, i.e. the indexes are stored according to the chronological order of the related voltages.

The buffer updating rules guarantees that the three voltage vectors are suitable to form a triplet.

The k-permutations of n base vectors are the different ordered arrangements of a k-element subset. In the present case, $n = 7$, $k = 3$ and the permutations are $n!/(n-k)! = 210$, so that the identification of the triplets is not trivial.

As a second step, one defines the *distance* as the *normalised* phase displacement between $\mathbf{u}^z(t_1)$ and the other two voltage vectors of the buffer. The two distances are stored in a buffer $B_d = [d_1, d_2]$, where d_1 is the distance between $\mathbf{u}^z(t_1)$ and $\mathbf{u}^z(t_3)$, and d_2 is the distance between $\mathbf{u}^z(t_1)$ and $\mathbf{u}^z(t_2)$. The distances are calculated according to an anticlockwise positive direction and they are defined only in the set $[-2; -1; 0; 1; 2; 3]$. With reference to Fig. 6, with a voltage buffer $\mathbf{u}^z(t_1) = \mathbf{u}^1$, $\mathbf{u}^z(t_2) = \mathbf{u}^6$ and $\mathbf{u}^z(t_3) = \mathbf{u}^3$, the buffer of distances is $B_d = [2, -1]$.

The sequence identification process is shown in Fig. 7. It can manage all possible combination, including the special case of a zero-voltage vector in the three-element buffer . The remaining sequences can be identified by defining simple rules on the distances in the three-element buffers. For example, the sequence 1 is identified when one of following rule applies to the buffer B_d:

$$|d_1|, |d_2| \leq 2 \quad \text{and} \quad d_1 d_2 = 2 \quad \text{or} \quad d_1 d_2 = -1 \tag{8}$$

Sequence 2 is detected by the rule:

$$d_1 d_2 = -2 \quad \text{or} \quad d_1 = 3 \quad \text{or} \quad d_2 = 3 \tag{9}$$

The use of the distances to identify the sequence results in a computationally fast method. Only a handful of *if* statements is necessary to carry out the sequence identification, allowing the algorithm implementation even on basic microprocessors.

The sequence identification process is shown in Fig. 7. It manages all possible combinations, including the special case of a zero-voltage vector in the three-element buffer.

B. Current variations reconstruction

The vectorial relationships between the magnitude of the current variations can be calculated for each sequence. The mathematical equations are reported in Table I. A practical example of LUTs updating is reported in [17]. For instance, one may consider the buffer of voltages equal to $(\mathbf{u}^4(k-2), \mathbf{u}^2(k-1), \mathbf{u}^1(k))$. The sequence identification procedure described in Sec. III-A result in the identification of sequence 2. Thus, the remaining four elements of the LUTs current variations, i.e. the ones corresponding to the voltage vectors

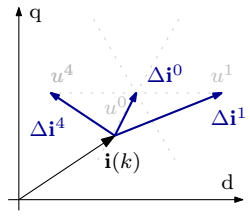

Fig. 8. Sequence 6 current variations representation.

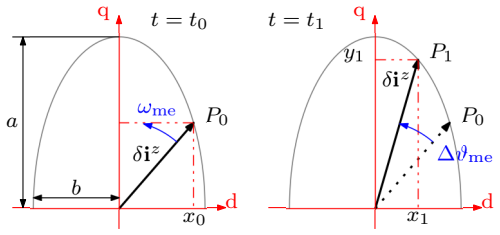

Fig. 9. Projections of a vector rotating at a constant speed when $L_q < L_d$

u^0, u^3, u^5 and u^6, can be updated by means of the calculations reported at the second row in TABLE I.

It is worth highlighting that sequence 6 does not allows the reconstruction of the remaining four elements. It represents a linearly dependent combination with two opposite active vectors and a zero voltage vector. Therefore, LUTs are not updated in that occurrences.

However, these combinations are still useful for the sake of current variations updating. For the sake of clarity, an example of sequence 6 $(1, 4, 0)$ and related current variations is reported in Fig. 8. The current variation $\Delta\mathbf{i}^0$ can be derived as the mean of the variations caused by the voltage vectors u^1 and u^4:

$$\Delta\mathbf{i}^0 = \frac{\Delta\mathbf{i}^1 + \Delta\mathbf{i}^4}{2} \tag{10}$$

The oldest current variation among $\Delta\mathbf{i}^0$, $\Delta\mathbf{i}^1$ and $\Delta\mathbf{i}^4$ is updated by a new value obtained by manipulating (10).

C. Compensation of the dq reference frame rotation

Let consider a steady state working condition. The forced current responses components $[\delta i_d^z\ \delta i_q^z]^T$ induced by the z-th stationary voltage vector are sinusoidal (7), as the z-th voltage dq projections $[\delta u_d^z\ \delta u_q^z]^T$. Moreover, during steady state operation, a current variation due to u^0 and measured at any $(k-m)$ step, with $m > 1$, is equal to the one measured at $(k-1)$, without any further approximation. These considerations can be used to compensate the effect of the rotor rotation on the estimated $\Delta\mathbf{i}^z$.

At every T_c, the current measurement updates the most recent element of the triplet. The remaining two elements are older, e.g. they could be 2, 3 or more control periods old. Therefore, the current reconstruction of all the other current variations by means of the technique proposed in this paper may be affected by an error if the position variation effect is not properly compensated. An effective and simple anti-ageing technique is proposed in this section.

The current variations due to active vectors are sinusoidal and they depend on the electromechanical position ϑ_{me}. Therefore, it is possible to correct them by taking advantage of this property. After the anti-age compensation, every element of the triplet will be considered to be one T_c old.

First of all, it is worth reminding that $\delta\mathbf{i}^0$ is supposed to be known. Thus, the forced response $\delta\mathbf{i}^z(k-1)$ can be extrapolated also in the model-free approach:

$$\delta\mathbf{i}^z(k-1) = \Delta\mathbf{i}^z(k-1) - \delta\mathbf{i}^0(k-1) \tag{11}$$

The rotations of the vectors $\mathbf{u}^z$ describe a circle in the dq voltage plane, whereas the rotations of vectors $\delta\mathbf{i}^z$ describe an ellipse in the dq current plane, due the motor magnetic anisotropy (Fig. 9). In particular, the ellipse semi-major axis of length a is placed along the lower inductance q-axis. The ellipse semi-minor axis of length b is thus placed along the d-axis.

The measured currents variations $\delta\mathbf{i}^z(k-m)$, with $m \geq 2$, can be used to calculate $\delta\mathbf{i}^z(k-1)$. Actually, the problem consists into estimating the future projections $(x_1(\vartheta_{\text{me}}), y_1(\vartheta_{\text{me}}))$ of a vector rotating at constant speed, starting from a previous position $(x_0(\vartheta_{\text{me}}), y_0(\vartheta_{\text{me}}))$ and knowing the time or angular displacement $\Delta\vartheta_{\text{me}}$ between the points (Fig. 9):

$$\Delta\vartheta_{\text{me}} = \omega_{\text{me}}(k-m+1)T_c \tag{12}$$

During each control period the motor speed is considered as a constant. In principle, the projections $(x_1 = \delta i_d^z(k-1), y_1 = \delta i_q^z(k-1)$ could be calculated as follows:

$$\delta i_d^z(k-1) = \delta i_d^z(k-m)\cos(\Delta\vartheta_{\text{me}}) - \delta i_q^z(k-m)\frac{a}{b}\sin(\Delta\vartheta_{\text{me}}) \tag{13}$$

A similar expression holds for the computation of $\delta i_q^z(k-1)$. Unfortunately, the ratio a/b is unknown, and it also depends on the current level that influences the motor magnetic saturation. Not excluding more sophisticated solutions, the easiest way is to neglect the term multiplied by the ratio, taking advantage of the fact that $\Delta\vartheta_{\text{me}}$ is very small in one control iteration. As a consequence, the projections can be approximated as follows:

$$\begin{cases} \delta i_d^z(k-1) \approx \delta i_d^z(k-2)\cos(\omega_{\text{me}}T_c) \\ \delta i_q^z(k-1) \approx \delta i_q^z(k-2)\cos(\omega_{\text{me}}T_c) \end{cases} \tag{14}$$

The compensation proposed in (14) was adopted in this paper. It is worth highlighting that the compensation requires the computation of just one cosine function and two multiplications.

IV. Results and Discussion

The experimental test bench adopted in this work consists of a SynR motor connected to an isotropic surface permanent magnet motor acting as a virtual load. Two different SynR motors were considered, whose plate data have been reported in TABLE II. The control drive algorithm was implemented in a *MicroLabBox* dSpace hardware. The control period T_c was set at $100\,\mu\text{s}$ and it corresponds to the updating time of the voltage vector output. The bus voltage was set at $300\,\text{V}$.

The schematic of the proposed model-free-based AC drive is reported in Fig. 10. The proposed model-free algorithm was also implemented in simulation to gain additional information

TABLE I
UPDATING RELATIONSHIPS FOR THE CURRENT VARIATIONS LUTS UPDATING

Sequence	Rule	Rule	Rule	Rule
Seq. 1	$\Delta\mathbf{i}^0 = \Delta\mathbf{i}^1 + \Delta\mathbf{i}^3 - \Delta\mathbf{i}^2$	$\Delta\mathbf{i}^4 = 2\Delta\mathbf{i}^0 - \Delta\mathbf{i}^1$	$\Delta\mathbf{i}^5 = 2\Delta\mathbf{i}^0 - \Delta\mathbf{i}^2$	$\Delta\mathbf{i}^6 = 2\Delta\mathbf{i}^0 - \Delta\mathbf{i}^3$
Seq. 2	$\Delta\mathbf{i}^0 = \frac{1}{2}(\Delta\mathbf{i}^1 + \Delta\mathbf{i}^4)$	$\Delta\mathbf{i}^3 = \Delta\mathbf{i}^2 + \Delta\mathbf{i}^4 - \Delta\mathbf{i}^0$	$\Delta\mathbf{i}^5 = 2\Delta\mathbf{i}^0 - \Delta\mathbf{i}^2$	$\Delta\mathbf{i}^6 = 2\Delta\mathbf{i}^0 - \Delta\mathbf{i}^3$
Seq. 3	$\Delta\mathbf{i}^4 = 2\Delta\mathbf{i}^0 - \Delta\mathbf{i}^1$	$\Delta\mathbf{i}^3 = \Delta\mathbf{i}^2 + \Delta\mathbf{i}^4 - \Delta\mathbf{i}^0$	$\Delta\mathbf{i}^5 = 2\Delta\mathbf{i}^0 - \Delta\mathbf{i}^2$	$\Delta\mathbf{i}^6 = 2\Delta\mathbf{i}^0 - \Delta\mathbf{i}^3$
Seq. 4	$\Delta\mathbf{i}^4 = 2\Delta\mathbf{i}^0 - \Delta\mathbf{i}^1$	$\Delta\mathbf{i}^2 = \Delta\mathbf{i}^1 + \Delta\mathbf{i}^3 - \Delta\mathbf{i}^0$	$\Delta\mathbf{i}^5 = 2\Delta\mathbf{i}^0 - \Delta\mathbf{i}^2$	$\Delta\mathbf{i}^6 = 2\Delta\mathbf{i}^0 - \Delta\mathbf{i}^3$
Seq. 5	$\Delta\mathbf{i}^0 = \frac{1}{3}(\Delta\mathbf{i}^1 + \Delta\mathbf{i}^3 + \Delta\mathbf{i}^5)$	$\Delta\mathbf{i}^2 = 2\Delta\mathbf{i}^0 - \Delta\mathbf{i}^5$	$\Delta\mathbf{i}^4 = 2\Delta\mathbf{i}^0 - \Delta\mathbf{i}^1$	$\Delta\mathbf{i}^6 = 2\Delta\mathbf{i}^0 - \Delta\mathbf{i}^3$

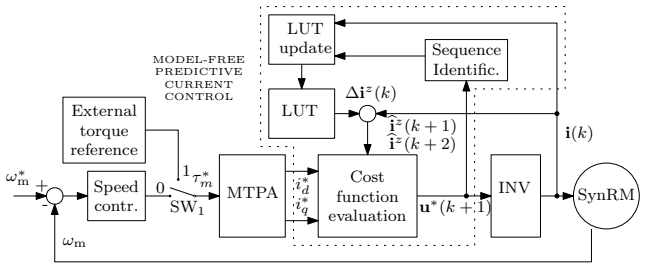

Fig. 10. Model-free predictive current control (dotted) in an electric drive. The state of switch SW$_1$ determines the drive operating conditions.

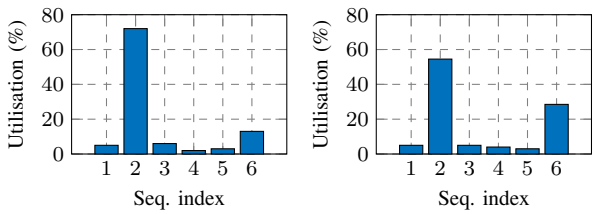

Fig. 11. Sequences during 1 s observation at steady-state and no load (simulation with motor SynRM$_1$, SW$_1 = 0$).

TABLE II
NAMEPLATE DATA OF THE MOTORS UNDER TEST

Motor Data	Symbol	SynRM$_1$	SynRM$_2$
Pole pairs	p	2	2
Phase resistance	R	16 Ω	4.7 Ω
Direct inductance	L_d	1 H	0.4 H
Quadrature inductance	L_q	0.3 H	0.08 H
Nominal current	I_N	3 A	5.6 A
Nominal speed	ω_N	500 rpm	1500 rpm
Nominal torque	τ_N	8.1 N m	10.2 N m

which ease the demonstration. The motor models implemented in the simulation were comprehensive of the magnetic saturations by means of LUTs as in Fig. 1.

In order to prove the feasibility of the proposed model-free approach, it is important to demonstrate the usefulness of the sequence identification. To this aim, several simulations were carried out and two different results are reported in the histograms of Fig. 11. The simulation was relative to motor SynRM$_1$ (Table II) and state SW$_1 = 0$ in Fig.10, i.e. with an active speed control loop, at steady state and no load. The remarkable utilisation of sequence 6 indicates the importance of considering also that sequence, neglected in [13]. The measured quantities are reported in *per unit* (p.u.) to ease the discussion and results comparisons. In particular, the currents were normalised with respect to $I_N/\sqrt{2}$ due to the adopted MTPA strategy. The speed measurements were normalised with respect to the rated value ω_N.

A. Anti-stagnation capability

The anti-stagnation capability of the model-free predictive current control with the reconstruction method described in Sec. III is evaluated for the motor named SynRM$_1$ (TABLE II). Two model-free predictive current control methods are compared: first the one proposed in [13], then the one presented in Sec. III. The quantisation of the current measurements was also implemented. The results are reported in Fig. 12. The former method suffers of small stagnation effects, which results in straight segments in Fig. 12 (top figure). Actually, it was found out that Seq. 6 was applied during those intervals. Under the same operating conditions, the simulation was repeated by implementing the proposed model-free algorithm that includes the sequence 6 and the rotation compensation. The results are reported at the bottom of Fig. 12, where the stagnation effect is effectively reduced and an example of LUT content is also highlighted. In the same figure, one can note the presence of small bumps, for example at $\vartheta_{\text{me}} \approx \pi/2$. It has been found that they depend on measurement noise in the currents. They may affect one or more $\Delta\mathbf{i}^z$ of the triplet that are used to estimate the current variations due to the remaining voltage vectors (not included in the triplet), according to TABLE I. The linear combinations of TABLE I can either emphasize or reduce the effects of the current errors (originally present in the measurements) and associated to a specific voltage vector in Fig.12. These bumps are transient situations that are readily fixed by the self-repairing feature of the model-free technique, within one electrical period of the rotor position. In other respects, the effect of bumps itself can be limited by both an higher switching and a more accurate current sensing.

B. Prediction error maps

This section discusses the current prediction error in different working conditions. Several simulations are carried out and the current prediction of the model-based and model-free schemes are obtained for both motors of TABLE II. The

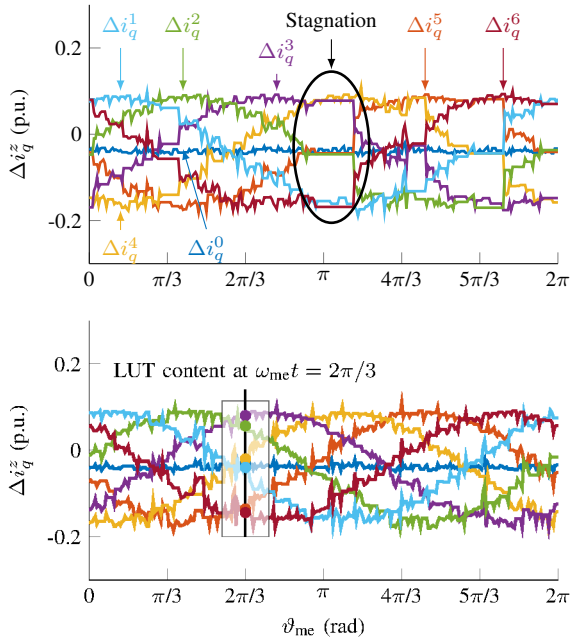

Fig. 12. Time evolution at constant speed of the LUT for the q-axis current without (top) and with (bottom) considering Seq. 6 (SynRM$_2$, simulation, SW$_1 = 0$).

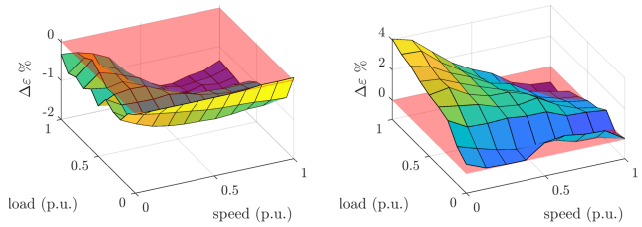

(a) SynRM$_1$ (b) SynRM$_2$

Fig. 13. Normalised difference of the prediction error between model-based and model-free (simulation, SW$_1 = 1$).

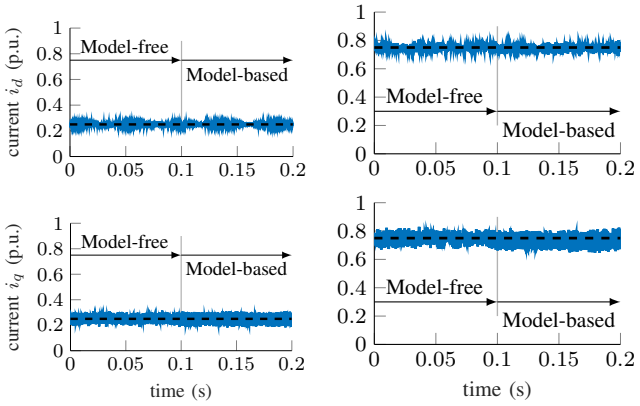

(a) $\tau_m^* = 25\%$ rated load (b) $\tau_m^* = 25\%$ rated load

Fig. 14. Comparison between model-based and model-free predictive current control at different load values and at $\omega_m = 25\%\,\omega_N$ (SynRM$_1$, experimental, SW$_1 = 1$).

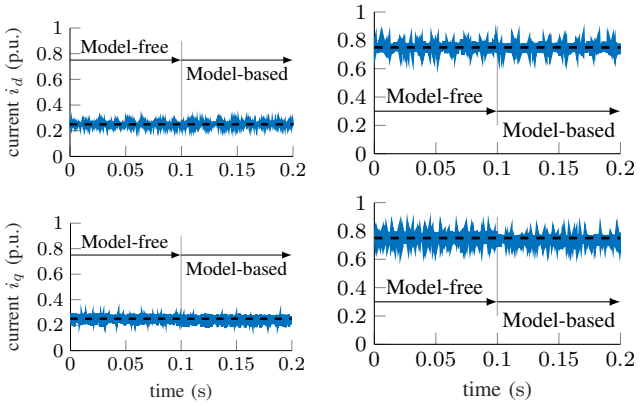

(a) $\tau_m^* = 25\%$ rated load (b) $\tau_m^* = 25\%$ rated load

Fig. 15. Comparison between model-based and model-free predictive current control at different load values and at $\omega_m = 75\%\,\omega_N$ (SynRM$_1$, experimental, SW$_1 = 1$).

prediction error is calculated as follows:

$$\varepsilon\% = \left\| \frac{\hat{\mathbf{i}}(k+1) - \mathbf{i}(k+1)}{I_N} \right\| \cdot 100 \tag{15}$$

Fig. 13 shows the normalised difference defined as:

$$\Delta\varepsilon\% = \varepsilon\%_{\text{model-based}} - \varepsilon\%_{\text{model-free}} \tag{16}$$

That is, a positive value (e.g. $\Delta\varepsilon = 2\%$) in a given normalised working point means that the prediction obtained by model-based control is worse of 2% with respect to the prediction obtained by model-free control. The comparisons were carried out for both SynRM$_1$ (Fig. 13a) and SynRM$_2$ (Fig. 13b). The results of Fig. 13a establishes that for SynRM$_1$ the model-based prediction is always better than the model-free one. Conversely, the result of Fig. 13b relative to SynRM$_2$ exhibits large portions of speed-torque plane (i.e. some working conditions) in which the model-free has a prediction error fairly lower than the model-based solution. This does not establish any superiority of a method over the other, also because a rather simple model with unsaturated inductances was used. But it leaves the way open to further investigations and improvements on both sides.

For a fair comparison, the model-based predictive current control should be supported by proper motor parameters self-commissioning procedures [8], [9], [18], [19] or online parameter estimator algorithms [20]–[22].

As regards the model-free technique, the major weak point is that the prediction relies on past measurement, and strongly depends on rotor position. At higher speed, the past measurements become quickly obsolete. The compensation described in Sec. III-C aims at reducing this flaw. Of course, the prediction error can be mitigated by increasing the switching frequency of the inverter, as proven in [17], by accepting increasing switching losses.

C. Results of steady-state tests

In this paper, a maximum torque-per-ampere (MTPA) control strategy is selected [23]. Neglecting on purpose any motor saturation, an approximated MTPA strategy yields equal current references, i.e. $i_d^* = i_q^*$. In polar coordinates, the MTPA trajectory has a constant angle equal to $45°$. Other choices are of course available, and in particular the one proposed in [24].

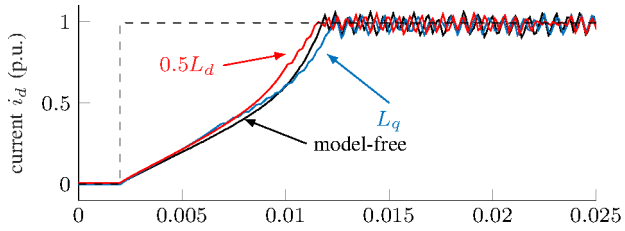

(a) Step on d-axis, $i_q^* = 0$

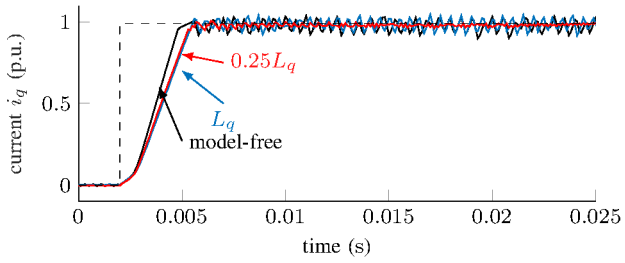

(b) Step on q-axis, $i_d^* = 0$

Fig. 16. Current measurements with different motor parameters (SynRM$_1$, experimental, SW$_1$ $= 1$, $\omega_{\rm m} = 0.25\,\omega_N$).

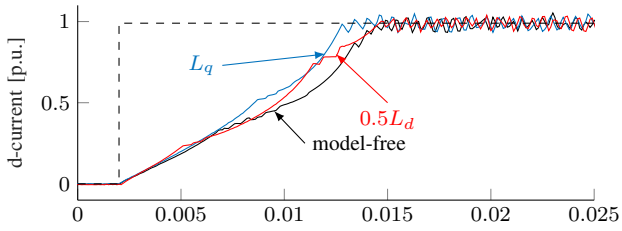

(a) Step on d-axis, $i_q^* = 0$

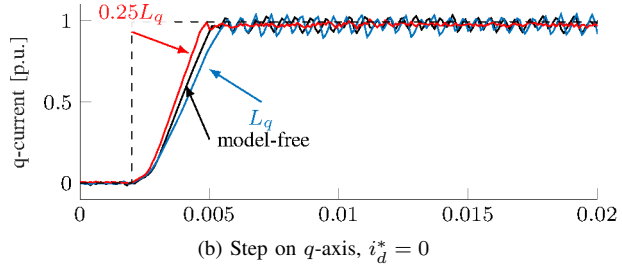

(b) Step on q-axis, $i_d^* = 0$

Fig. 17. Current measurements with different motor parameters (SynRM$_1$, experimental, SW$_1$ $= 1$, $\omega_{\rm m} = 0.75\,\omega_N$).

It is worth pointing out that there are MTPA techniques that do not require motor parameters knowledge, thus in favour of a full model-free electric drive. The resulting complete drive scheme is reported in Fig. 10.

Two different steady-state tests are carried out at various load levels and two speeds, namely 25% and 75% of the rated speed. The results are reported in Fig. 14 and 15, respectively.

During the tests, a switch from model-free and model-based predictive current control is performed. The operation at light load are reported in Fig. 14a and 15a: the transitions are smooth and there are almost no differences between the two control schemes. The obtained results are still comparable even at high load torque, as shown in Fig. 14b and 15b. On one hand, it can be seen that the model-free control exhibits a slightly higher current ripple at high speed. On the other hand, the model-based control suffers a dependence on the load torque, as expected from the discussion in Sec. IV-B.

D. Results of dynamic tests

The tests results reported in this section are obtained with the speed reference maintained by the load motor, while the motor under test is set to current control mode only (SW$_1$ $=$ 1). A current step is imposed to one of the dq-axes. Therefore, no torque is produced and the speed is not affected, allowing a fair comparison of the current responses between model-free and model-based approaches.

At the startup, the information stored in the current variations LUTs suffer of stagnation since no voltage vectors have been applied yet. However, as soon as one (random) voltage vector is applied on the motor, the LUTs information is updated as inherent feature of the proposed technique, just after 3 period T_c. A stable behaviour of the currents is then guaranteed even at the startup of the motor drive.

The current measurements obtained for SynRM$_1$ are reported in Fig. 16 and 17. The results of the model-based predictive current control are obtained by keeping the inductances in (3) at constant values reported in each figure. It is evident how the model-based predictive current control transients are influenced by parameter mismatches, whereas the model-free scheme simply has no parameters to tune. And despite its simplicity, the model-free control guarantees a benchmarking dynamic performances.

To test the generality of the conclusions, the same experiment is carried out with motor SynRM$_2$, which presents a rather different motor parameters set (see Table II). The results are reported in Fig. 18 and 19. As the model-based control, it was verified that the proposed model-free control allows operations in the full speed and torque ranges.

The results confirm that almost identical behaviour in the dynamic are obtained by model-free and model based predictive controls. The steady state current ripple is worst in the model-free scheme compared to the case when the model-based predictive current control adopts the correct value for the inductances. However, this aspect of the model-free approach could be improved by proper design of a specific cost function in (1).

V. Conclusion

An improved finite-set model-free predictive current control of a synchronous reluctance motor drive is proposed in this paper. The current control is obtained without any knowledge of the motor parameters and therefore it is insensible to any parameters mismatch. The steady state and dynamic performances are slightly inferior, but very similar, to those obtained by a model-based scheme. The solution may be convenient in those cases where the motor manufacturer does not provide enough motor data and self-commissioning procedures are difficult (or not convenient) to realise.

The relationship between the last three applied voltage vectors are exploited to reconstruct all possible current variations, which are necessary for the predictive algorithm. The main improvements are in both the efficient algorithm for the triplet

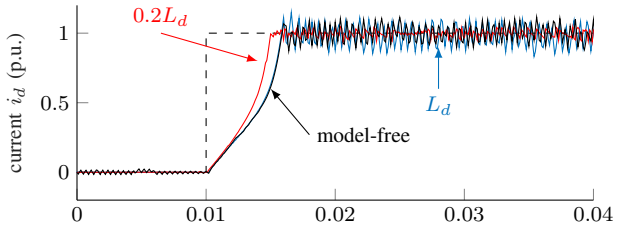

(a) Step on d-axis, $i_q^* = 0$

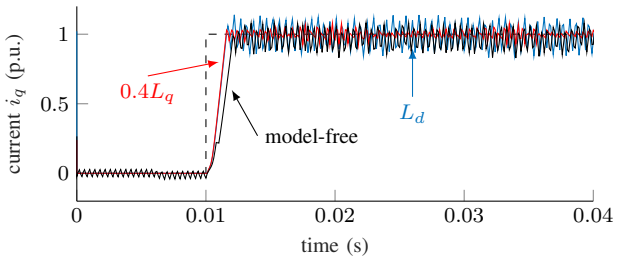

(b) Step on q-axis, $i_d^* = 0$

Fig. 18. Current measurements with different motor parameters (SynRM$_2$, experimental, SW$_1$ = 1, $\omega_m = 0.25\,\omega_N$).

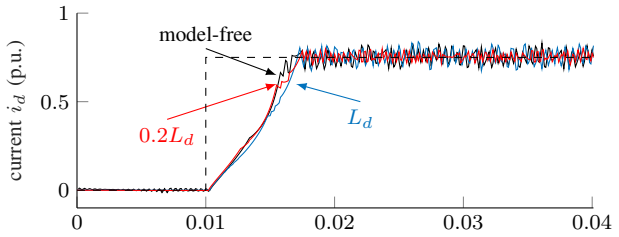

(a) Step on d-axis, $i_q^* = 0$

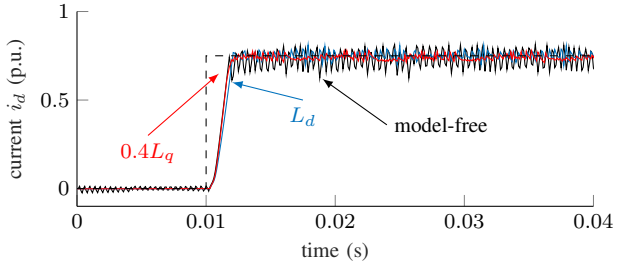

(b) Step on q-axis, $i_d^* = 0$

Fig. 19. Current measurements with different motor parameters (SynRM$_2$, experimental, SW$_1$ = 1, $\omega_m = 0.75\,\omega_N$).

identification and the compensation of the position change over time in the control horizon.

The proposed model-free predictive current control requires a very small computational power in comparison with the conventional model-based if one considers all motor parameters of (3). If a very basic model-based technique with constant and known parameters is adopted, thus neglecting every saturation and temperature effect, the two computational requirements would be comparable, smoothing the way for the technological transfer of this interesting control technique to the industrial application.

The validity of the algorithm has been proven by means of ad-hoc tests carried out on an experimental rig. Performances of model-free and model-based scheme have been compared and discussed in details.

References

[1] T. Geyer, *Model Predictive Control of High Power Converters and Industrial Drives*, 1st ed. Wiley, 2016.

[2] J. Rodriguez and P. Cortes, *Predictive Control of Power Converters and Electrical Drives*, 1st ed. Wiley, 2012.

[3] S. Bolognani, S. Bolognani, L. Peretti, and M. Zigliotto, "Design and implementation of model predictive control for electrical motor drives," *IEEE Trans. Ind. Electron.*, vol. 56, no. 6, pp. 1925–1936, June 2009.

[4] M. Preindl, "Robust control invariant sets and Lyapunov-based MPC for IPM synchronous motor drives," *IEEE Trans. Ind. Electron.*, vol. 63, no. 6, pp. 3925–3933, June 2016.

[5] R. Antonello, M. Carraro, L. Peretti, and M. Zigliotto, "Hierarchical scaled-states direct predictive control of synchronous reluctance motor drives," *IEEE Trans. Ind. Electron.*, vol. 63, no. 8, pp. 5176–5185, Aug 2016.

[6] S. Wendel, A. Dietz, and R. Kennel, "FPGA based finite-set model predictive current control for small PMSM drives with efficient resource streaming," in *2017 IEEE International Symposium on Predictive Control of Electrical Drives and Power Electronics (PRECEDE)*, Sept 2017, pp. 66–71.

[7] L. Ortombina, F. Tinazzi, and M. Zigliotto, "Magnetic modeling of synchronous reluctance and internal permanent magnet motors using radial basis function networks," *IEEE Trans. Ind. Electron.*, vol. 65, no. 2, pp. 1140–1148, Feb 2018.

[8] L. Peretti, P. Sandulescu, and G. Zanuso, "Self-commissioning of flux linkage curves of synchronous reluctance machines in quasi-standstill condition," *IET Electric Power Applications*, vol. 9, no. 9, pp. 642–651, 2015.

[9] M. Hinkkanen, P. Pescetto, E. Mölsä, S. E. Saarakkala, G. Pellegrino, and R. Bojoi, "Sensorless self-commissioning of synchronous reluctance motors at standstill without rotor locking," *IEEE Trans. Ind. Appl.*, vol. 53, no. 3, pp. 2120–2129, May 2017.

[10] S. Nalakath, M. Preindl, and A. Emadi, "Online multi-parameter estimation of interior permanent magnet motor drives with finite control set model predictive control," *IET Electric Power Applications*, vol. 11, no. 5, pp. 944–951, 2017.

[11] C. K. Lin, T. H. Liu, J. t. Yu, L. C. Fu, and C. F. Hsiao, "Model-free predictive current control for interior permanent-magnet synchronous motor drives based on current difference detection technique," *IEEE Trans. Ind. Electron.*, vol. 61, no. 2, pp. 667–681, Feb 2014.

[12] C. K. Lin, J. t. Yu, Y. S. Lai, and H. C. Yu, "Improved model-free predictive current control for synchronous reluctance motor drives," *IEEE Trans. Ind. Electron.*, vol. 63, no. 6, pp. 3942–3953, June 2016.

[13] D. Da Rú, M. Polato, and S. Bolognani, "Model-free predictive current control for a SynRM drive based on an effective update of measured current responses," in *2017 IEEE International Symposium on Predictive Control of Electrical Drives and Power Electronics (PRECEDE)*, Sept 2017, pp. 119–124.

[14] T. Geyer, "Algebraic tuning guidelines for model predictive torque and flux control," *IEEE Trans. Ind. Appl.*, vol. 54, no. 5, pp. 4464–4475, Sept 2018.

[15] P. Zanchetta, "Heuristic multi-objective optimization for cost function weights selection in finite states model predictive control," in *2011 Workshop on Predictive Control of Electrical Drives and Power Electronics*, Oct 2011, pp. 70–75.

[16] J. Falck, G. Buticchi, and M. Liserre, "Thermal stress based model predictive control of electric drives," *IEEE Trans. Ind. Appl.*, vol. 54, no. 2, pp. 1513–1522, March 2018.

[17] S. Bolognani, P. Carlet, F. Tinazzi, and M. Zigliotto, "Fast and robust model free predictive current control for synrel motor drives," in *2018 IEEE Energy Conversion Congress and Exposition (ECCE)*, Sept 2018.

[18] S. A. Odhano, P. Pescetto, H. A. A. Awan, M. Hinkkanen, G. Pellegrino, and R. Bojoi, "Parameter identification and self-commissioning in AC motor drives: a technology status review," *IEEE Trans. Power Electron.*, pp. 1–1, 2018.

[19] N. Bedetti, S. Calligaro, and R. Petrella, "Stand-still self-identification of flux characteristics for synchronous reluctance machines using novel saturation approximating function and multiple linear regression," *IEEE Trans. Ind. Appl.*, vol. 52, no. 4, pp. 3083–3092, July 2016.

[20] R. Antonello, L. Ortombina, F. Tinazzi, and M. Zigliotto, "Online stator resistance tracking for reluctance and interior permanent magnet synchronous motors," *IEEE Trans. Ind. Appl.*, vol. 54, no. 4, pp. 3405–3414, July 2018.

[21] G. Feng, C. Lai, and N. C. Kar, "A novel current injection-based online parameter estimation method for PMSMs considering magnetic saturation," *IEEE Trans. Magn.*, vol. 52, no. 7, pp. 1–4, July 2016.
[22] M. Pulvirenti, G. Scarcella, G. Scelba, A. Testa, and M. Harbaugh, "Online stator resistance and permanent magnet flux linkage identification on open-end winding PMSM drives," *IEEE Trans. Ind. Appl.*, pp. 1–1, 2018.
[23] S. Kim, Y. D. Yoon, S. K. Sul, and K. Ide, "Maximum torque per ampere (MTPA) control of an IPM machine based on signal injection considering inductance saturation," *IEEE Trans. Power Electron.*, vol. 28, no. 1, pp. 488–497, Jan 2013.
[24] L. Ortombina, F. Tinazzi, and M. Zigliotto, "Adaptive maximum torque per ampere control of synchronous reluctance motors by radial basis function networks," *IEEE Journal of Emerging and Selected Topics in Power Electronics*, pp. 1–1, 2018.

Paolo Gherardo Carlet Paolo Gherardo Carlet received the B.S. degree and M.S. degree (hons.) in electrical engineering in 2015 and 2017, respectively, from the University of Padova, Padova, Italy. He is currently working toward the Ph.D. degree with the Electrical Drives Laboratory, University of Padova. He joined the Department of Electrical Engineering, University of Padova, as an Associate Researcher where he worked in the synchronous motor drives field. His main interests include sensorless and predictive control for ac motor drives.

Fabio Tinazzi (M '16) received the B.S. and M.S., Ph.D. degree in Mechatronic Engineering from University of Padova in 2008, 2011 and 2015 respectively. Since February 2017, he is a Researcher at the Department of Management and Engineering, University of Padova, Vicenza, Italy. His main research interests include sensorless control, predictive control and parameter estimation techniques for ac motors.

Silverio Bolognani (M'98, SM'16, F'2019) received the Laurea degree in Electrical Engineering from the University of Padova, Italy, in 1976. He is author of more than 250 publications about design and control of electrical drives for land and marine propulsion, energy generation and conversion, home appliances, automotive, industry, etc. He was Head of the Department of Electrical Engineering from 2001 to 2008, and vice-Rector for the Research from 2009 to 2015 at the Padova University. He is currently a Full Professor of Electrical Converters, Machines and Drives. He is the Chairman of the IEEE IAS/IES/PELS North Italy Joint Chapter and Member of the Scientific Committee of National and International conferences and associations.

Mauro Zigliotto (M '98, SM '18) is a native of Vicenza, Italy. He is full professor of Electrical Machines and Drives at University of Padova, Italy and head of the Electric Drives Laboratory in Vicenza, Italy. Advanced control strategies and self-commissioning for ac motors are Prof. Zigliotto's main research interests. He is the secretary of the IEEE IAS-IES-PELS North Italy Joint Chapter.